Journal of Machine Engineering, 2026, Vol. 26,
ISSN 1895-7595 (Print) ISSN 2391-8071 (Online)

Received*: 12 March 2026* / Accepted: *30 March 2026* / Published online: *16 April 2026*

microstructures, mechanical property,
high-strength steel,
wire arc additive manufacturing

Manh-Tung DO[1], Quang Huy HOANG[1],
Van Thao LE[2], Van Tuan NGUYEN[3*],
Xuan Nang HO[4], Van Hiep PHAM[3],
Trung Nam PHAM[3], Van Anh NGUYEN[5]

EVALUATION OF MECHANICAL PROPERTIES AND MICROSTRUCTURE OF HIGH-STRENGTH STEEL WALLS FABRICATED BY WIRE ARC ADDITIVE MANUFACTURING

This study investigates the microstructural and mechanical characteristics of a high-strength steel thin wall fabricated via wire arc additive manufacturing (WAAM). A 20-layer wall was produced using a bidirectional deposition strategy with fixed processing parameters to ensure repeatability. Microstructural analysis revealed significant spatial heterogeneity along the build direction. The bottom region exhibited the finest grain size (0.96±0.23 μm) due to the substrate heat sink effect, while the top region reveals the coarsest grain size (1.84±0.36 μm) due to slower cooling rates. XRD analysis confirmed the deposited material consists entirely of the ferrite phase. Mechanical testing showed a microhardness gradient ranging from 256±17.04 HV0.1 at the top to 288±16.78 HV0.1 at the bottom that directly correlates with grain refinement. Tensile tests revealed exceptional performance with ultimate tensile strength (UTS) exceeding 980 MPa, yield strength (YS0.2%) in range of 560–620 MPa, and elongation above 20%, meeting industrial requirements for structural applications. Fracture surface morphology confirmed a ductile micro-void coalescence mechanism, indicating high plastic deformation capability. These results demonstrate the WAAM capability to produce high-strength, structurally reliable steel components, supporting its application in large-scale manufacturing for shipbuilding, heavy engineering, and load-bearing structural systems.

1. INTRODUCTION

Wire arc additive manufacturing (WAAM) is an emerging metal additive manufacturing (AM) approach that employs metallic wire as the feed material and an electric arc to melt and deposit the wire during processing [1, 2]. In this technique, three-dimensional components are formed through the successive deposition of molten material onto a substrate in a layer-

[1] Faculty of Mechanical Engineering, Le Quy Don Technical University, Vietnam
[2] Advanced Technology Center, Le Quy Don Technical University, Vietnam
[3] Faculty of Mechanical Engineering and Mechatronics, PHENIKAA University, Vietnam
[4] Faculty of Vehicle & Energy Engineering, PHENIKAA University, Vietnam
[5] Institute of sustainable manufacturing, University of Kentucky, United States
[*] E-mail: tuan.nguyenvan@phenikaa-uni.edu.vn
https://doi.org/10.36897/jme/220151

by-layer manner, following predefined deposition paths [3, 4]. Various welding-based power sources can be integrated into the WAAM process, including plasma-arc welding (PAW), gas-metal-arc welding (GMAW), cold-metal transfer (CMT), and gas-tungsten-arc welding (GTAW) [5, 6]. The material deposition is typically carried out using either industrial robotic manipulators or multi-axis CNC platforms to ensure precise control and repeatability [7]. Compared with powder-based metal AM technologies that rely on laser energy, WAAM offers significantly higher deposition rates (approximately 4–8 kg/h), improved material utilization efficiency, and substantially reduced equipment and feedstock costs [8]. Owing to these advantages, WAAM has become well suited for the fabrication of large-scale components across various industrial fields, including automotive, aerospace, marine and shipbuilding, construction and infrastructure, oil and gas, and tooling industries [7]. A broad spectrum of metallic materials can be processed using WAAM, such as high-strength steels, stainless steels, aluminum alloys, titanium alloys, and nickel-based superalloys [3, 9].

Among these materials, high-strength steels containing low carbon and modest alloying additions are especially attractive due to their favorable weldability, high strength, good fracture toughness, and cost-effectiveness [10]. Consequently, these steels have attracted considerable research interest in WAAM applications, particularly for marine and shipbuilding structures [11]. Previous investigations on WAAM-fabricated high strength steels have primarily focused on understanding the influence of thermal history and processing parameters on microstructural development and mechanical performance. For example, Bourlet et al. [12] studied ER100 steel walls produced by WAAM and reported a refined microstructure consisting of coarse allotriomorphic ferrite along with retained austenite.

Their work also revealed pronounced anisotropy in mechanical properties, with hardness values ranging from approximately 220 to 280 HV2 and tensile strengths spanning about 520 to 790 MPa depending on the sampling location. Fang et al. [13] investigated an 800-MPa-class steel component fabricated by GMAW-based WAAM and demonstrated that a predominantly martensite/bainite microstructure can be achieved, leading to a favorable strength-ductility-toughness balance. Recent work by Liu et al. [14] investigated the microstructural evolution and anisotropic mechanical behaviour of ER100S-G steel fabricated via WAAM, combining experimental characterization with finite-element thermal simulations. Their results demonstrated that interlayer dwell time strongly influences thermal accumulation, phase distribution, and tensile performance, leading to pronounced property variations along the build direction.

Although WAAM of high-strength steels has been extensively studied, limited work has systematically linked thermal cycling–induced microstructural gradients with directional mechanical behavior and isotropy in thin-wall structures. The present study provides a comprehensive evaluation of ER110S-G steel fabricated by WAAM, combining detailed microstructural characterization, phase and compositional analysis, and mechanical testing in both the building and transverse directions. By establishing clear process-microstructure-property relationships and demonstrating near-isotropic high-strength performance, this work offers new insights into the structural reliability of WAAM-fabricated high-strength steel components for large-scale industrial applications.

The outcomes of this work are expected to provide a deeper insight into the structure-property relationships governing high strength steel walls. From an industrial perspective, this study contributes to establishing process–microstructure-property linkages that are essential for predicting performance, ensuring mechanical consistency, and optimizing process parameters for large-scale structural applications.

2. MATERIALS AND METHODS

In this research, the feedstock material employed was SM110 welding wire (Hyundai Welding), which is classified under the AWS standard as ER110S-G steel. The wire has a diameter of 1.2 mm, and its chemical composition is given in Table 1. The substrate is made of carbon steel (DIN-C45 - equivalent to AISI 1045) with dimensions of 200 mm x 200 mm x 10 mm (width x length x thickness) that was cut from a large plate. The substrate material is a medium carbon steel, and its chemical elements are presented in Table 1, offering good strength, machinability, and wear resistance. Owing to these properties, C45 steel is widely employed in mechanical components such as shafts, gears, and structural parts, making it a suitable base material for the WAAM deposition process investigated in this study. The substrate surface for the deposition of the thin wall was ground and cleaned to eliminate the oxidation layer and contamination.

Table 1. Chemical composition of the welding wire and substrate materials (in wt.%)

Element	Mo	Ni	Cr	Mn	Si	C	P	S	Fe
Welding wire	0.58	1.95	0.34	1.90	0.80	0.089	0.010	-	Bal.
Substrate	-	-	-	0.50–0.80	0.15–0.35	0.42–0.50	≤ 0.045	≤ 0.35	Bal.

The thin wall investigated in this study was fabricated using a GMAW-WAAM system, which is composed of a six-axis industrial robot (Panasonic TM-1400WGIII), a GMAW power source, and an automatic wire feeder (Fig. 1a). The robotic arm manipulated the welding torch to deposit molten metal layer by layer onto the substrate to form the thin wall. During WAAM, repeated melting causes partial dilution between the first layer (ER110S-G steel) and the substrate (DIN-C45 steel), allowing alloying elements such as Mn and Si to enrich the deposited layers. This alloying, combined with thermal cycling–induced grain refinement, leads to solid-solution strengthening and improved hardness and tensile strength

The thin wall (Fig. 1c) was manufactured using a bidirectional deposition strategy (Fig. 1b). Each layer consisted of alternating welding and non-welding travel paths to control heat input and maintain geometric stability. The welding direction was reversed between adjacent layers to minimize residual stress accumulation and distortion. A total of 20 layers were deposited sequentially to achieve the target wall height. The length of the printed wall was programmed at 100 mm. The interlayer dwell time was kept constant at 60 s. All process parameters, including welding current (I), voltage (U), and torch travel speed (v), were maintained at fixed values during fabrication to ensure repeatability: I = 151 A, U = 20 V, and v = 32 cm/min, as shown in Table 2.

Table 2. The process parameters of WAAM used for the deposition of the wall

Parameter	Value and unit
Welding current - *I*	151 A
Arc voltage - *U*	20 V
Travel speed - *v*	32 cm/min
Dwell time between two successive layers	60 s
Distance from the contact tip to the workpiece	15 mm
Flow rate of the shielding gas	15 L/min

These process parameters were selected based on a prior optimization study, which aimed at achieving stable deposition, uniform bead geometry, and defect-free thin-wall fabrication, as shown in Fig. 1c. A detailed parametric analysis of heat input effects on microstructures and properties will be separately investigated in our future work. During the deposition, a mixed gas of 80% argon and 20% carbon dioxide with a flow rate of 15 L/min was utilized for shielding the molten pool.

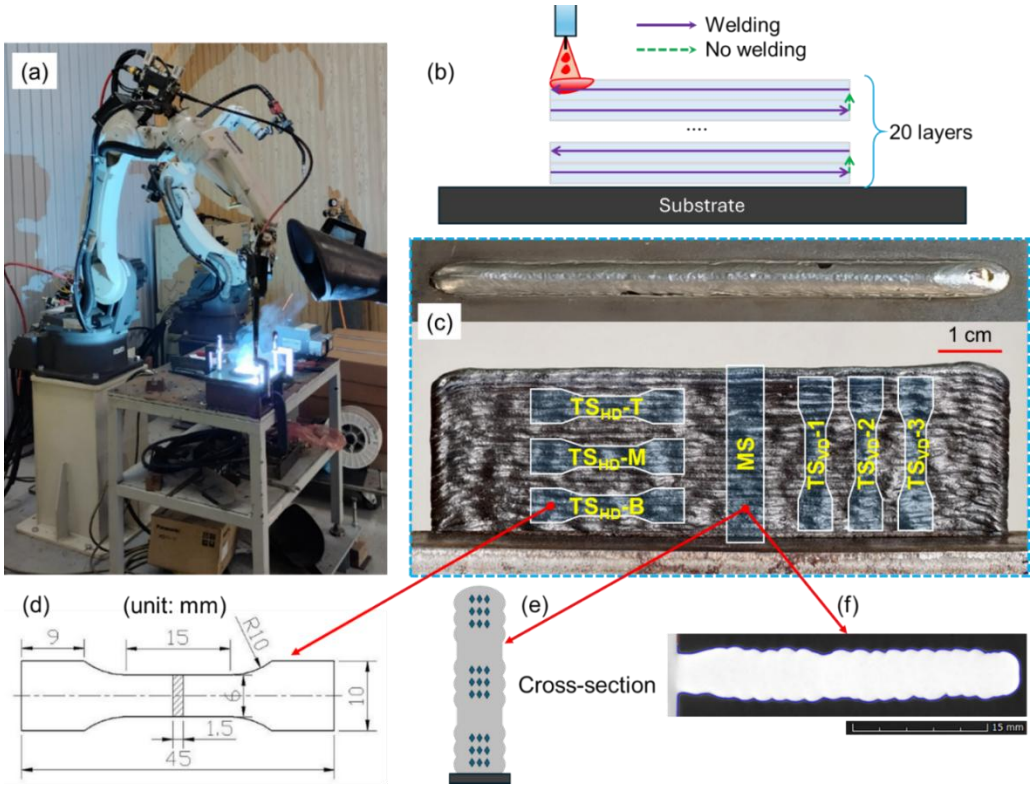

Fig. 1. (a) The GMAW-AM robot, (b) the deposition method of the thin wall, (c) the weld bead and thin wall fabricated with the optimal process parameters and positions to extract tensile testing samples (TSHD and TSVD) and the metallographic sample (MS), (d) the dimensions of tensile testing samples, (e) locations for measuring microhardness, and (f) X-ray CT scanning of the MS sample

To characterize the microstructural and mechanical characteristics of the deposited metal, a metallographic specimen (MS) and tensile specimens in the horizontal direction (i.e., TSHD-T in the top, TSHD-M in the middle, and TSHD-B in the bottom region) and in the

vertical direction (i.e., TSVD-1, TSVD-2, and TSVD-3) were extracted from the built wall (Fig. 1c) using an EDM machine. The horizontal tensile specimens were extracted from different height locations along the build direction to evaluate the effect of thermal history on mechanical properties. The geometry and dimensions of the tensile specimens were designed according to the ASTM E8/E8M standard (Fig. 1d). The tensile tests were executed at room temperature on a tensile test machine (INSTRON 3T). The displacement speed of the tensile crosshead was 10 mm/min. After the tensile tests, the fractured surface morphologies of the tensile specimens were captured using an SEM machine (Hitachi SU3500).

The cut surfaces of the MS sample were subsequently processed by grinding, polishing, and chemical etching operations for the microstructure and microhardness tests. The microstructure was captured by a digital optical microscope and a SEM machine. Hardness tests were executed with a Vickers tester. A 980.7 mN in load and an idle time of ten seconds were utilized in a test. The hardness was tested in the three regions of the cross-section (bottom, middle, and top) with nine measurements in each region (Figure 1e). Moreover, the X-ray CT scanning technique was employed to examine the internal structure and defect distribution of the MS specimens (Fig. 1f).

In the current study, the thermal evolution during the WAAM deposition of the wall was simulated using a three-dimensional finite element model implemented in LS-DYNA. The progressive material deposition was represented through element activation following the torch path. The moving heat input was modeled using the Goldak double-ellipsoidal heat source to describe the spatial heat distribution in the front and rear regions of the arc, as presented in [14]. The temperature-dependent thermal properties of high-strength ER110S-G steel reported in [15] were considered, and heat transfer through conduction, convection, and radiation was included in the simulation model. The 20-layer wall and substrate were modeled according to the thin wall geometry as in the experiment (Fig. 1c). To evaluate heat accumulation and cooling rate variation during deposition, thermal cycles were extracted at representative build heights – i.e., the middle points of the second layer (L-2), the tenth layer (L-10), and the 18th layer (L-18). The description of the developed thermal simulation model can be found in our previous study [16].

3. RESULTS AND DISCUSSION

3.1. MARCRO AND MICROSTRUCTURE ANALYSIS

The macroscopic morphology of the deposited wall (Fig. 1c) demonstrates uniform bead stacking and consistent layer geometry, indicating stable material transfer and adequate interlayer bonding throughout the build. Furthermore, the X-ray CT scanning results on the MS sample (Fig. 1f) reveal a dense internal structure with no observable lack of fusion between adjacent layers and an absence of significant porosity or volumetric defects. The minimal defect population suggests that the selected WAAM process parameters provided sufficient heat input and molten pool stability to promote complete metallurgical bonding and gas escape during solidification. This high internal integrity is critical for achieving the enhanced mechanical performance reported in this study.

Figure 2 illustrates the microstructural characteristics and their evolution along the build direction of the deposited wall that reveal clear spatial heterogeneity between the top, middle, and bottom regions. Such variations are typical of WAAMed walls and arise primarily from differences in thermal history, cooling rate, and cyclic reheating during layer-by-layer deposition.

As shown in Fig. 3a, elevated temperatures progressively extend upward as successive layers are deposited, indicating reduced heat dissipation away from the melt pool. The thermal cycles in Figure 3b further demonstrate a systematic decrease in cooling rate from the lower to upper layers, with the second layer (L-2) exhibiting the highest cooling rate (83 °C/s), followed by intermediate values at the tenth layer (L-10) (58 °C/s) and the lowest rate at the top region (the 18th layer (L-18), about 52 °C/s). It should be noted that the thermal histories predicted by simulations have not been experimentally validated using in-situ thermocouple measurements, which may introduce some uncertainty in the quantitative accuracy. Nevertheless, the observed cooling rate trend is consistent with findings reported in previous studies [16, 17], supporting the reliability of the present results.

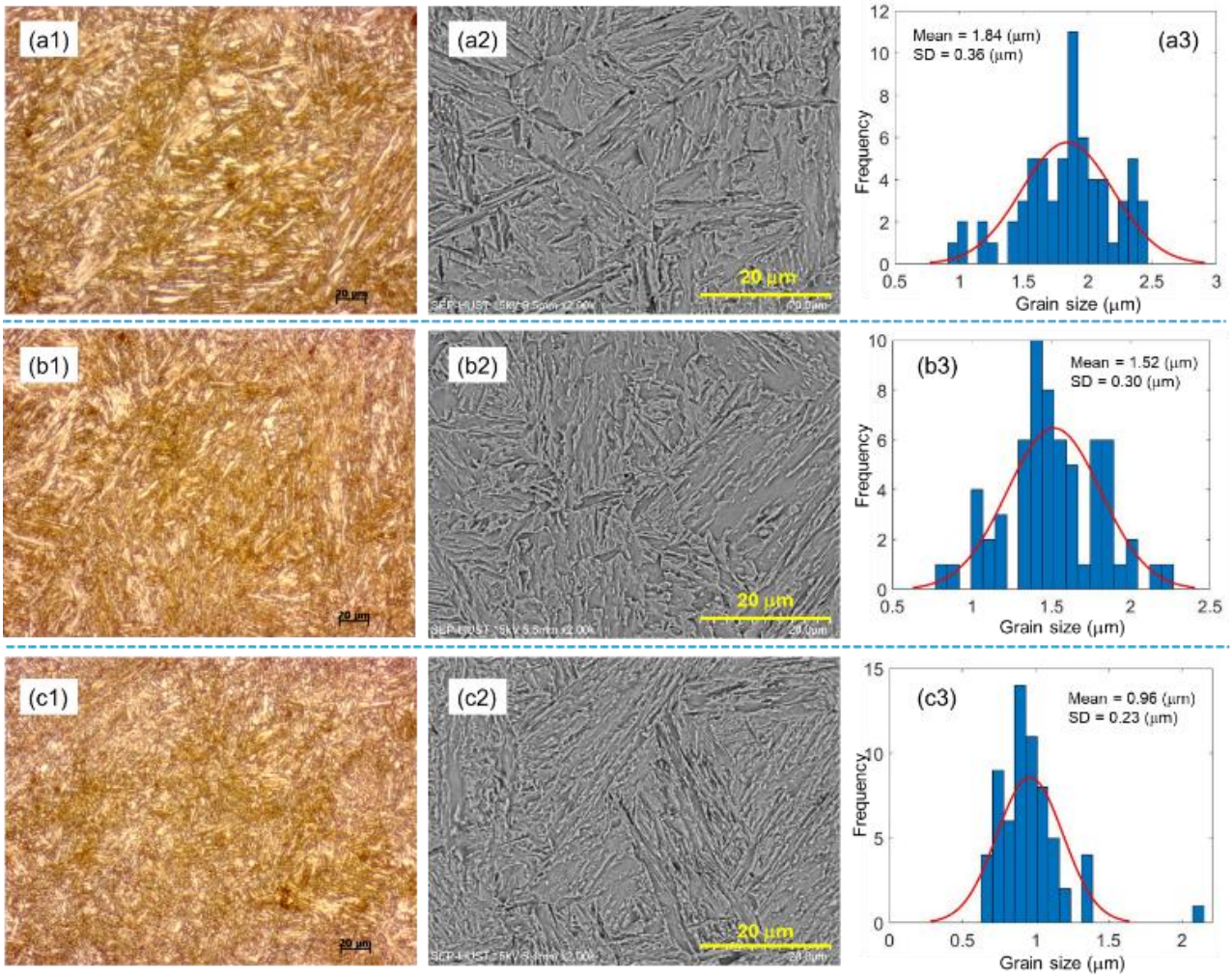

Fig. 2. Microstructure of the wall in different zones: (a1)-(b1)-(c1) optical images, (a2)-(b2)-(c2) SEM images, and (a3)-(b3)-(c3) grain size distribution in the top, middle, and bottom, respectively

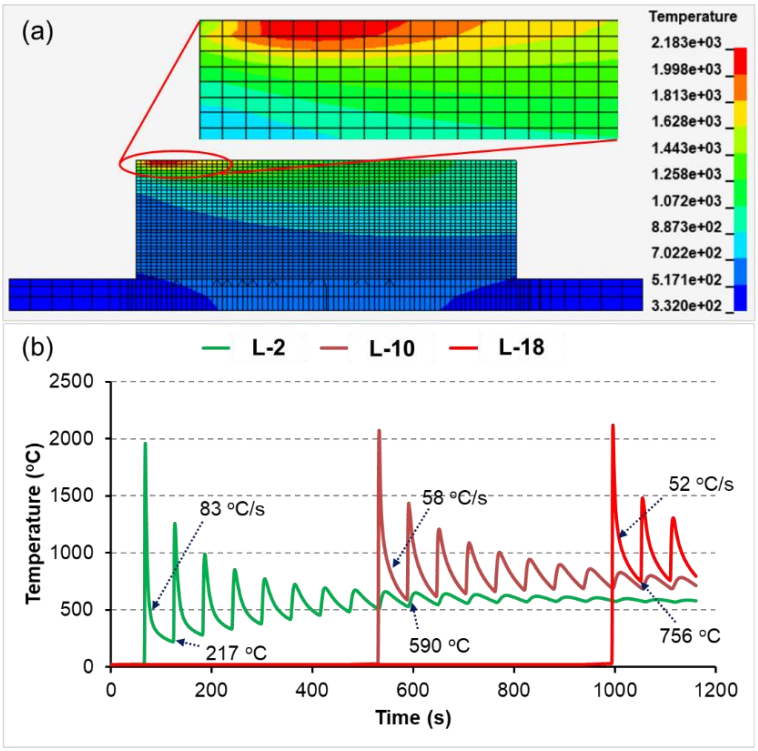

Fig. 3. Thermal simulation results during the deposition of the wall: (a) thermal distribution in the wall during the deposition and (b) the thermal cycle at the middle points of the second layer (L-2), the tenth layer (L-10), and the 18th layer (L-18)

This gradual reduction in cooling rate is attributed to diminished substrate heat sink effects and increased thermal accumulation within the deposited material, which directly influences microstructural coarsening toward the upper layers of the wall [16, 17]. Consequently, the top region exhibits a relatively coarse microstructure with elongated lath-like features, as observed in both optical and SEM images (Fig. 2a1 and Fig. 2a2). The corresponding grain size distribution (Fig. 2a3) shows the largest mean grain size (1.84±0.36 μm) and the highest standard deviation, indicating a broader grain size dispersion.

In contrast, the middle region demonstrates a noticeably refined and more homogeneous microstructure (Fig. 2b1 and Fig. 2b2). The grain size distribution (Fig. 2b3) shows a reduced mean grain size (1.52±0.30 μm) with a narrower spread. This refinement is associated with the repeated thermal cycling caused by subsequent layer deposition above, which induces partial austenitization followed by rapid cooling [18]. Such cyclic reheating acts as an in-situ heat treatment, enhancing nucleation rates and suppressing excessive grain growth, leading to a more uniform microstructure.

The bottom region presents the finest microstructure among all examined zones, with a mean grain size of approximately 0.96 μm (Fig. 2c3). SEM observations (Fig. 2c2) reveal densely packed, fine lath structures. This is due to a high cooling rate and strong thermal gradients near the substrate. The substrate acts as an efficient heat sink during the initial deposition stages, resulting in rapid solidification and significant grain refinement. Additionally, the bottom region undergoes the highest number of thermal cycles, further contributing to microstructural homogenization and grain refinement through repeated phase transformations.

The XRD analysis results (Fig. 4) also indicate that the deposited wall is mainly characterized by ferrite phase. The four peaks α-(110), α-(200), α-(211), and α-(220) were observed. In XRD patterns, the peaks related to oxides were not found. Indeed, no distinct oxides or inclusions were observed within the resolution limits of SEM and XRD used in the current study, indicating that any oxides present are likely in very low quantities and below the detection limits of both SEM and XRD. The absence of oxide peaks in XRD also indicates the effectiveness of the shielding gas mixture (80% argon + 20% CO_2) used during deposition.

Theoretically, the solid-state transformation of high strength steels includes the following steps: First, austenite phase is formed and developed from the liquid state during the solidification period from 1300°C to 800°C. Thereafter, the transformation from austenite into bainite and ferrite phases occurs when the temperature is cooled down from 800 to 500°C [19]. Allotriomorphic ferrite is formed at prior austenite grains' boundaries. After that acicular ferrite may be nucleated at austenite/ferrite boundaries. In the final cooling period to room temperature, the remaining austenite may be partially or fully transformed into bainite and martensite, depending on the carbon content [18]. However, in the current study, under the WAAM processing conditions, the microstructure is primarily ferritic (as shown in Fig. 4).

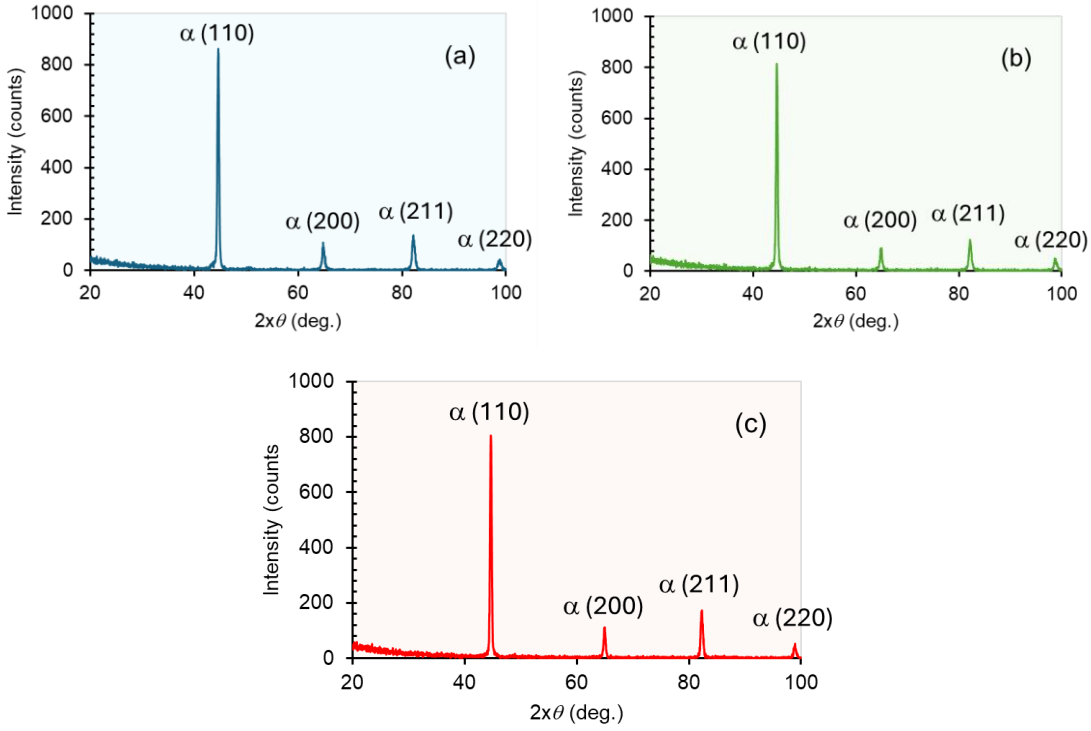

Fig. 4. XRD phase analysis in (a) the top, (b) the middle, and (c) the bottom of the wall

3.2. MECHANICAL PROPERTY ANALYSIS

Figure 5 shows the microhardness variation along the building direction of the wall. A clear gradient in hardness is observed, with the highest average microhardness measured in the bottom region, followed by the middle region, while the top region exhibits the lowest

hardness. The average microhardness is 288±16.78 HV0.1 in the bottom, 275±19.48 HV0.1 in the middle, and 256±17.04 HV0.1 in the top. This trend reflects the non-uniform thermal history inherent to the WAAM process and is closely correlated with the observed microstructural evolution along the build height. The bottom region exhibits the highest microhardness, which can be attributed to its refined microstructure and rapid cooling conditions during the initial deposition stages. The substrate acts as an effective heat sink, leading to high cooling rates that promote the formation of fine lath structures and potentially harder transformation products. In addition, the bottom layers experience multiple thermal cycles from subsequent deposition, which can further refine the microstructure through repeated phase transformations and tempering effects, contributing to enhanced hardness.

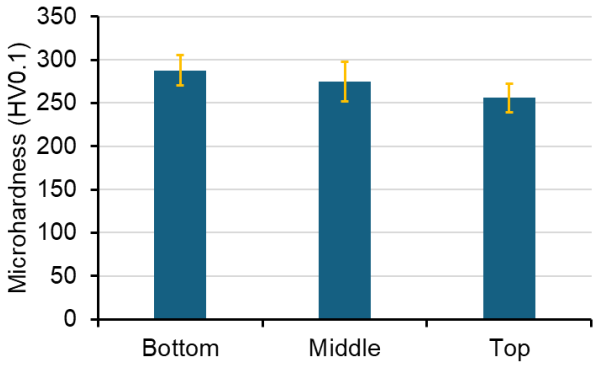

Fig. 5. Microhardness in various regions of the deposited wall

The middle region shows slightly reduced but relatively uniform microhardness values. This region undergoes repeated reheating and partial remelting, resulting in a balance between microstructural refinement and thermal softening. The combination of refined grain size and moderated cooling rates leads to stable hardness values with relatively small scatter, indicating good mechanical consistency in this zone. In contrast, the top region exhibits the lowest microhardness. This reduction is primarily associated with slower cooling rates due to limited heat dissipation and the absence of reheating from subsequent layers. These conditions favor grain coarsening and reduced dislocation density, leading to lower resistance to indentation. Furthermore, the lack of thermal cycling limits the refinement mechanisms active in the lower regions. The results obtained on microhardness are in line with the microstructure evolution. These results also emphasize the importance of process parameter optimization and thermal management strategies to achieve more uniform mechanical properties in additively manufactured structural components

Figure 6 presents the tensile stress–strain responses and the corresponding mechanical properties of the specimens tested along the horizontal direction (HD) and vertical direction (VD). As shown in Fig. 6a and 6b, all specimens exhibit a typical continuous yielding behavior without a distinct yield plateau, followed by pronounced strain hardening prior to fracture. The average tensile properties shown in Fig. 6c demonstrate that the WAAM-fabricated wall achieves high strength and good ductility. The ultimate tensile strength (UTS) exceeds 980 MPa in both loading directions, while the 0.2% yield strength ($YS_{0.2\%}$) ranges between approximately 560 and 620 MPa. These values meet the typical strength requirements for HSLA steels and are comparable to or higher than those reported for conventionally

manufactured counterparts. Furthermore, the elongation to failure remains above 20% for both HD and VD specimens, indicating a favorable strength-ductility balance that is essential for structural applications.

A degree of tensile anisotropy is observed between the two loading directions. The HD specimens exhibit slightly higher elongation and tensile strengths (YS and UTS) compared to the VD specimens. Nevertheless, the relatively small differences in tensile properties between HD and VD directions indicate strong metallurgical bonding between layers and effective fusion during deposition. The low mechanical anisotropy observed in Figure 6c can be attributed to the relatively homogeneous and refined microstructure developed during deposition.

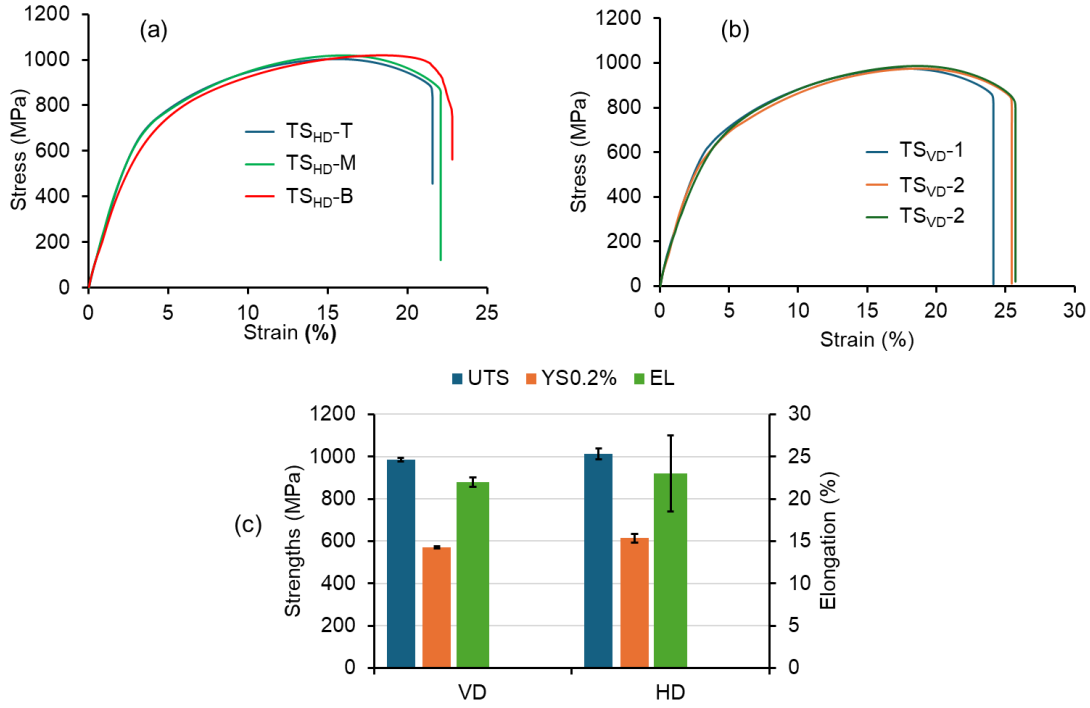

Fig. 6. (a) Stress-strain curves of the tensile test specimens in the horizontal direction (HD) and (b) Stress-strain curves of the tensile test specimens in the vertical direction (VD), and (c) the average values of UTS (MPa), YS0.2% (MPa) and elongation (EL%) of tensile specimens

Overall, the tensile results confirm that WAAM can be successfully employed to fabricate HSLA steel walls with high strength, good ductility, and limited anisotropy. These results demonstrate the WAAM capacity for fabricating load-bearing steel parts for industrial applications, where reliable mechanical performance in multiple loading directions is required.

4. SUMMARY

This study was undertaken to systematically investigate the microstructural characteristics, chemical homogeneity, and mechanical performance of an HSLA steel wall fabricated by GMAW-WAAM. By focusing on the evolution of properties along the building

height, the research aimed to provide deeper insights into the structure-property relationships and establish process-microstructure-property linkages necessary for the industrial adoption of WAAM in heavy engineering and shipbuilding. Based on the experimental results, the following conclusions are drawn:

- Microstructures of the wall show a significant spatial heterogeneity along the build direction. The bottom region exhibited the finest microstructure (0.96 μm) due to the substrate's heat sink effect and repeated thermal cycles, while the top region was the coarsest (1.84 μm) due to slower cooling rates and limited reheating.
- The microhardness gradient of the built wall directly correlates with the microstructural refinement, ranging from 288 HV0.1 at the bottom to 256 HV0.1 at the top. Tensile testing demonstrated high mechanical reliability, with ultimate tensile strength (UTS) exceeding 980 MPa and elongation above 20%, meeting industrial standards for HSLA steels.
- While horizontal specimens showed slightly higher strength and ductility than vertical ones, the overall limited anisotropy indicates effective fusion and strong metallurgical bonding between the deposited layers.
- Fracture surfaces reveal a high density of dimples across all regions, confirming that the material fails via a ductile micro-void coalescence mechanism.

In future work, we will focus on incorporating in-situ thermal measurements to validate the thermal simulation models. Moreover, systematic investigations of varying heat input parameters and interlayer temperature control will be conducted to further optimize structural uniformity and minimize residual stresses. Long-term performance evaluation, including fatigue and impact testing, will also be considered to support the broader industrial implementation of GMAW-WAAM for critical load-bearing applications.

ACKNOWLEDGEMENT

This study is funded by Phenikaa University under the grant number PU2023-1-A15.

REFERENCES

[1] COSTELLO S.C.A., CUNNINGHAM C.R., XU F., SHOKRANI A., DHOKIA V., NEWMAN S.T., 2023, *The State-Of-The-Art of Wire Arc Directed Energy Deposition (WA-DED) As an Additive Manufacturing Process for Large Metallic Component Manufacture,* International Journal of Computer Integrated Manufacturing, 36/3, 469–510, https://doi.org/10.1080/0951192X.2022.2162597.

[2] BALIDAS A., KERBRAT O., HASCOET J.-Y., 2024, *The Potential of Additive Manufacturing of Metal Components to Reduce Environmental Impacts*, Journal of Machine Engineering, 24/2, 94–104, https://doi.org/10.36897/jme/186988.

[3] SRIVASTAVA M., RATHEE S., TIWARI A., DONGRE M., 2023, *Wire Arc Additive Manufacturing of Metals: A Review on Processes, Materials and Their Behaviour*, Materials Chemistry and Physics, 294, 126988, https://doi.org/10.1016/j.matchemphys.2022.126988.

[4] RAUCH M., HASCOET J.-Y., ROUSSEAU C., RUCKERT G., 2021, *Thermal Monitoring for Metallic Additive Manufacturing Multi-Beads Multi-Layers Parts*, Journal of Machine Engineering, 32/3, 167–186, https://doi.org/10.36897/jme/139158.
[5] SALEH B., FATHI R., TIAN Y., RADHIKA N., JIANG J., MA A., 2023, *Fundamentals and Advances of Wire Arc Additive Manufacturing: Materials, Process Parameters, Potential Applications, and Future Trends*, Springer, London.
[6] REMY A., NWANKPA U., RAUCH M., HASCOËT J.-Y., RUCKERT G., 2024, *Impact of a Variation in Wire Feed Speed on Deposits from the Wire Arc Additive Manufacturing (WAAM)*, Journal of Machine Engineering, 24/2, 117–128, https://doi.org/10.36897/jme/188308.
[7] ZHANG H., LI R., LIU J., WANG K., WEIJIAN Q., SHI L., 2024, *State-Of-Art Review on the Process-Structure-Properties-Performance Linkage in Wire Arc Additive Manufacturing*, Virtual and Physical Prototyping, 19/1, 1–45, https://doi.org/10.1080/17452759.2024.2390495.
[8] PUSATERI V., OLSEN S.I., HAUSCHILD M.Z., KARA S., 2023, *Potential for Absolute Sustainability of Wire-Arc Additive Manufacturing: A Boat Propellers Case*, CIRP Annals, 72/1, 29–32, 2023, https://doi.org/10.1016/j.cirp.2023.04.034.
[9] NGUYEN V.C., LE V.T., PHAM N.-L., NGUYEN A.-T., 2023, *Multi-Objective Optimization for Weld Track Geometry in Wire-Arc Directed Energy Deposition of ER308L Stainless Steel*, Journal of Machine Engineering, 23/2, 123–134, https://doi.org/10.36897/jme/166134.
[10] BALUCH N., UDIN Z.M., ABDULLAH C.S., 2014, *Advanced High Strength Steel in Auto Industry: An Overview*, Engineering, Technology & Applied Science Research, 4/4, 686–689, https://doi.org/10.48084/etasr.444.
[11] GHAZALI S.N.M., et al., 2025, *A Focused Review on Numerical Computation in Wire Arc Additive Manufacturing for High Strength Low Alloy Steels: Past Insights and Potential Opportunities*, The International Journal of Advanced Manufacturing Technology, 141/5–6, 2679–2708, https://doi.org/10.1007/s00170-025-16817-9.
[12] BOURLET C., ZIMMER-CHEVRET S., PESCI R., BIGOT R., ROBINEAU A., SCANDELLA F., 2020, *Microstructure and Mechanical Properties of High Strength Steel Deposits Obtained by Wire-Arc Additive Manufacturing*, Journal of Materials Processing Technology, 285, 116759, https://doi.org/10.1016/j.jmatprotec.2020.116759.
[13] FANG Q., et al., 2022, *Microstructure and Mechanical Properties of 800-MPa-Class High-Strength Low-Alloy Steel Part Fabricated by Wire Arc Additive Manufacturing*, Journal of Materials Engineering and Performance, 31/9, 7461–7471, https://doi.org/10.1007/s11665-022-06784-7.
[14] LIU Q., WANG L., LIU J., CHEN L., WEI Y., TIAN Y., 2026, *Investigation of Microstructure and Mechanical Properties of High-Strength Low-Alloy Steel Fabricated by Wire and Arc Additive Manufacturing*, JOM, 10/2, 216, https://doi.org/10.1007/s11837-025-08080-w.
[15] MISHRA V., BABU A., SCHREURS R., WU K., HERMANS M.J.M., AYAS C., 2023, *Microstructure Estimation and Validation of ER110S-G Steel Structures Produced by Wire and Arc Additive Manufacturing*, Journal of Materials Research and Technology, 23, 3579–3601, https://doi.org/10.1016/j.jmrt.2023.01.214.
[16] LE V.T., et al., 2022, *Influences of the Process Parameter and Thermal Cycles on the Quality of 308L Stainless Steel Walls Produced by Additive Manufacturing Utilizing an Arc Welding Source*, Welding in the World, 66/8, 1565–1580, https://doi.org/10.1007/s40194-022-01330-4.
[17] LE V.T., BUI M.C., NGUYEN T.D., NGUYEN V.A., NGUYEN V.C., 2022, *On the Connection of the Heat Input to the Forming Quality in Wire-And-Arc Additive Manufacturing of Stainless Steels*, Vacuum, 209, 111807, https://doi.org/10.1016/j.vacuum.2023.111807.
[18] RODRIGUES T.A., DUARTE V., AVILA J.A., SANTOS T.G., MIRANDA R.M., OLIVEIRA J.P., 2019, *Wire and Arc Additive Manufacturing of HSLA Steel: Effect of Thermal Cycles on Microstructure and Mechanical Properties*, Additive Manufacturing, 27, 440–450, https://doi.org/10.1016/j.addma.2019.03.029.
[19] SHI Y., HAN Z., 2024, *Effect of Weld Thermal Cycle on Microstructure and Fracture Toughness of Simulated Heat-Affected Zone for a 800 MPa Grade High Strength Low Alloy Steel*, Journal of Materials Processing Technology, 207/1–3, 30–39, , https://doi.org/10.1016/j.jmatprotec.2007.12.049.